International Journal of Nanomedicine

Dovepress
open access to scientific and medical research

Open Access Full Text Article

ORIGINAL RESEARCH

Molecular Imaging of Matrix Metalloproteinase-2 in Atherosclerosis Using a Smart Multifunctional PET/MRI Nanoparticle

Yingfeng Tu[1,2], Xiaowei Ma[3], Hao Chen[2,4], Yuhua Fan[5], Lei Jiang[2], Ruiping Zhang[2,6], Zhen Cheng[2,4]

[1]Department of Cardiology, The First Affiliated Hospital of Harbin Medical University, Harbin, Heilongjiang, People's Republic of China; [2]Molecular Imaging Program at Stanford, Department of Radiology and Bio-X Program, Stanford University, Stanford, CA, USA; [3]Department of Nuclear Medicine, The Second Xiangya Hospital, Central South University, Changsha, Hunan, People's Republic of China; [4]Molecular Imaging Center, Shanghai Institute of Materia Medica, Chinese Academy of Sciences, Shanghai, People's Republic of China; [5]College of Pharmacy, Harbin Medical University, Daqing, Heilongjiang, People's Republic of China; [6]The Third Hospital of Shanxi Medical University, Shanxi Bethune Hospital, Shanxi Academy of Medical Sciences, Taiyuan, People's Republic of China

Correspondence: Zhen Cheng, Molecular Imaging Program at Stanford, Department of Radiology and Bio-X Program, Canary Center at Stanford for Cancer Early Detection, 1201 Welch Road, Lucas Expansion, P095, Stanford University, Stanford, CA, 94305, USA, Tel +01-650-723-7866, Email zcheng@simm.ac.cn; Ruiping Zhang, Department of Radiology, the Third Hospital of Shanxi Medical University, Shanxi Bethune Hospital, Shanxi Academy of Medical Sciences, Taiyuan, 030032, People's Republic of China, Email 1900547207@qq.com

Background: Matrix metalloproteinases from macrophages are important intraplaque components that play pivotal roles in plaque progression and regression. This study sought to develop a novel multifunctional positron emission tomography (PET) and magnetic resonance imaging (MRI) contrast agents based on MMP-2 cleavable nanoparticles to noninvasive assessment of MMP-2 activity in mouse carotid atherosclerotic plaques.

Results: Macrophage-rich vascular lesions were induced by carotid ligation plus high-fat diet and streptozotocin-induced diabetes in CL57/BL6 mice. To render iron oxide nanoparticles (IONP) specific for the extracellular MMP-2, the magnetic nanoparticle base material has been derivatized with 1,4,7-triazacyclononane-1,4,7-triacetic acid (NOTA) for the nuclear tracer ^{64}Cu labeling and the MMP-2-cleavable peptide modified with polyethylene glycol 2000, yielding a multi-modality reporter (^{64}Cu-NOTA-IONP@MMP2c-PEG2K, MMP2cNPs) for PET/MR imaging. Small animal PET imaging and biodistribution data revealed that MMP2cNPs exhibited remarkable plaque uptake (3.06 ± 0.87% ID/g and 1.83 ± 0.28% ID/g at 4 and 12 h, respectively). And MMP2cNPs were rapidly cleared from the contralateral normal carotid artery, resulting in excellent plaque-to-normal carotid artery contrasts. Furthermore, in vivo MRI showed a preferential accumulation of MMP2cNPs in atherosclerotic lesions compared with the non-cleavable reference compound, MMP2ncNPs. In addition, histological analyses revealed iron accumulations in the carotid atherosclerotic plaque, in colocalization with MMP-2 expression and macrophages.

Conclusion: Using a combination of innovative imaging modalities, in this study, we demonstrate the feasibility of applying the novel smart MMP2cNPs as a PET/MR hybrid imaging contrast agent for detection of MMP-2 in atherosclerotic plaque in vivo.

Keywords: atherosclerosis, macrophage, matrix metalloproteinase-2, nanoparticles, magnetic resonance imaging, positron emission tomography

Introduction

Despite current optimal treatment, atherosclerosis diseases are still the leading cause of death all over the world.[1] Nowadays, there has been a shift in emphasis from treatment of atherosclerosis diseases to the primary or secondary prevention of diseases. Furthermore, advances in atherosclerotic plaque biology have translated into the discovery of novel therapies, which in turn have led to a reduction in morbidity and mortality. However, this shift puts forward new challenges to basic research as well as to clinical practice and further stimulates technological revolution of existing imaging diagnostic methods. In recent years, nanotechnology is emerging as a new field of interdisciplinary research, cutting across the disciplines of materialogy, biology, chemistry, engineering, and medicine, which is expected to lead to

Received: 4 September 2022
Accepted: 9 November 2022
Published: 28 December 2022

Graphical Abstract

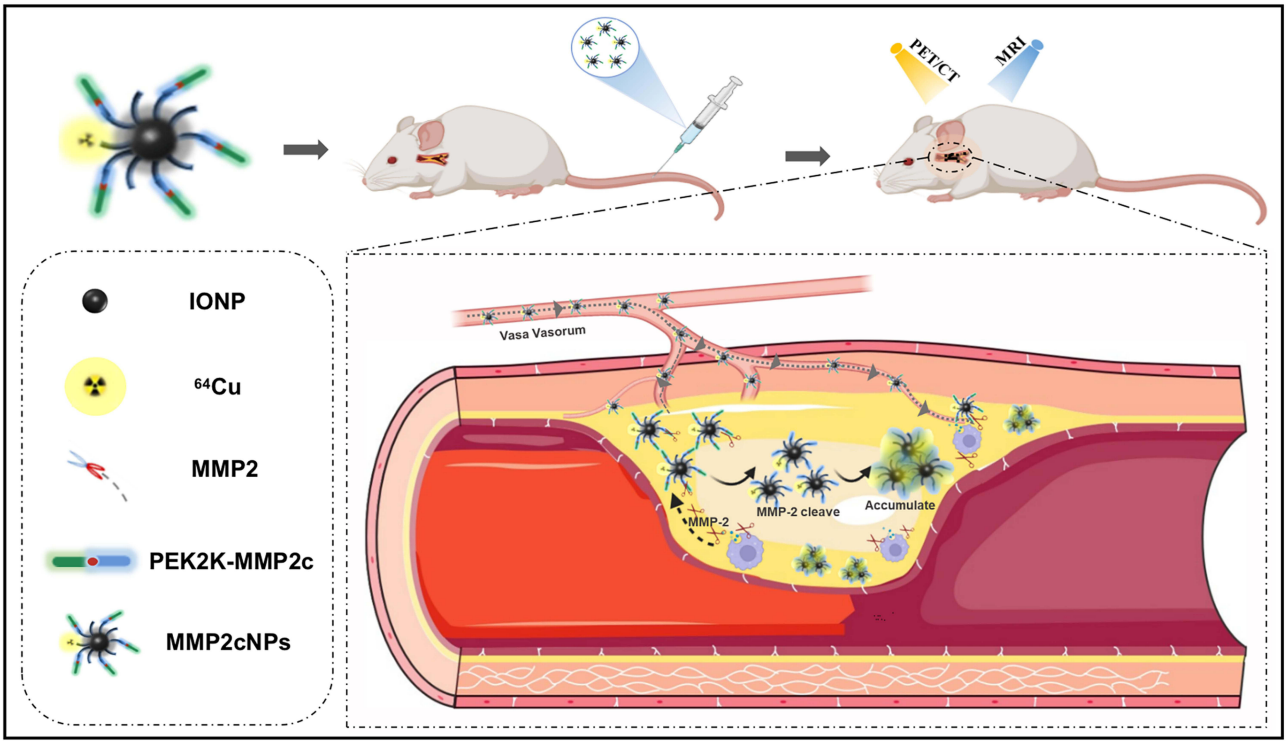

major advances in atherosclerosis detection, diagnosis, and clinical treatment.[2–5] As potentially powerful probes, nanoparticles (NPs) have been widely applied to molecular imaging in biological and clinical diagnostics,[5–7] which are generally believed to revolutionize clinical bioimaging techniques in cardiovascular diseases, especially in atherosclerosis. Inflammation in atherosclerosis contributes to all stages of atherosclerosis, which contributes importantly to initiation, maturation, and instability of atherosclerotic plaques.[8,9] Monocyte-derived macrophages can induce collagen breakdown in the fibrous cap of human atherosclerosis by producing MMP-2.[10] With the deepening of the research on MMP-2, Seifert et al confirmed that MMP-2 activities were significantly higher in the ApoE-/- cuff model in unstable atherosclerotic plaques as compared to downstream more stable plaque phenotypes.[11] In clinical studies, Dhillon et al also identified MMP-2 as an independent predictor of all-cause mortality.[12] These studies have indicated that MMP-2 facilitates plaque rupture and clinical events. Therefore, assessment of MMP-2 activation in atherosclerotic plaques in vivo can provide novel insight into the pathogenesis of vascular disease and serve as a clinical tool for evaluation of vascular inflammation, for determination of individualized therapeutic strategies, and for monitoring the effects of therapeutic interventions.

The rapidly evolving field of molecular imaging based on nanotechnology will ultimately allow us to accurately assess the components of atherosclerotic lesions at molecular and cellular levels.[13,14] It may enable the detection of biological markers, such as macrophages, vascular cell adhesion protein 1 (VCAM-1), and vascular endothelial growth factor receptor 2 (VEGFR-2), whose expression is directly related to the pathophysiological status of atherosclerotic plaque.[15–18] On the basis of the avidity of macrophages for polysaccharide-containing supramolecular structures such as nanoparticles, Weissleder et al developed a novel trimodality nanoparticle to directly monitor macrophages in atherosclerotic plaques.[19] Recently, ultrasmall superparamagnetic iron oxide (USPIO) particles functionalized with R832 and R826, two peptides specifically recognizing VCAM-1 and apoptosis, respectively, have been demonstrated to hold potential for the detection of atherosclerotic plaques by delivering nanoparticles specifically to VCAM-1-expressing and

apoptotic cells within atherosclerotic plaques.[15] Burtea et al demonstrated that their novel VCAM-1 and apoptotic cell targeted USPIO derivatives seemed to be highly promising tools for atherosclerosis imaging contributing to the detection of vulnerable plaques.[15] Recently, Kiugel et al evaluated a gallium-68 labeled peptide for the detection of MMP-2/9 in atherosclerotic mouse aorta. They disclosed that the MMP-2/9-targeting ^{68}Ga-DOTA-TCTP-1 showed specific uptake in inflamed atherosclerotic lesions.[20] In addition, in a recent study, Zheng et al developed a CD81-(cluster of differentiation 81 protein-) targeted microparticles of iron oxide (CD81-MPIO) for magnetic resonance imaging (MRI) of the murine atherosclerosis.[21]

Nanoprobes are also being tested for multi-modal approaches. Unlike other molecular imaging modalities, the combination of positron emission tomography (PET) or single-photon emission computed tomography (SPECT) with MRI can offer synergistic advantages for non-invasive, sensitive, high-resolution, and quantitative imaging, which is suitable for early detection of various diseases such as atherosclerosis in vivo.[22,23] Here, we report the development of novel MMP-2-cleavable PET/MRI agents based on IONP. We conjugated MMP-2-cleavable peptide modified with polyethylene glycol 2000 (PEG2K-MMP2c) to USPIO and radiolabeled with ^{64}Cu, yielding a smart multi-modality reporter ^{64}Cu-NOTA-IONP@MMP2c-PEG2K (MMP2cNPs) to monitor the MMP-2 expression within atherosclerosis via PET and MR imaging in vivo (Figure 1). We hypothesize that the novel MMP2cNPs accumulation in carotid plaque correlates with the expression level of MMP-2, and that in vivo PET signal correlates with inflammatory plaque components identified by in vivo MRI and in vitro immunohistochemical staining.

Materials and Methods

General

2,2′-(7-(2-((2,5-dioxopyrrolidin-1-yl) oxy)-2-oxoethyl)-1,4,7-triazonane-1,4-diyl) diacetic acid (NOTA-NHS ester) was purchased from CheMatech. N-hydroxysuccinimide (NHS) and N-hydroxysulfosuccinimide (sulfo-NHS) was purchased

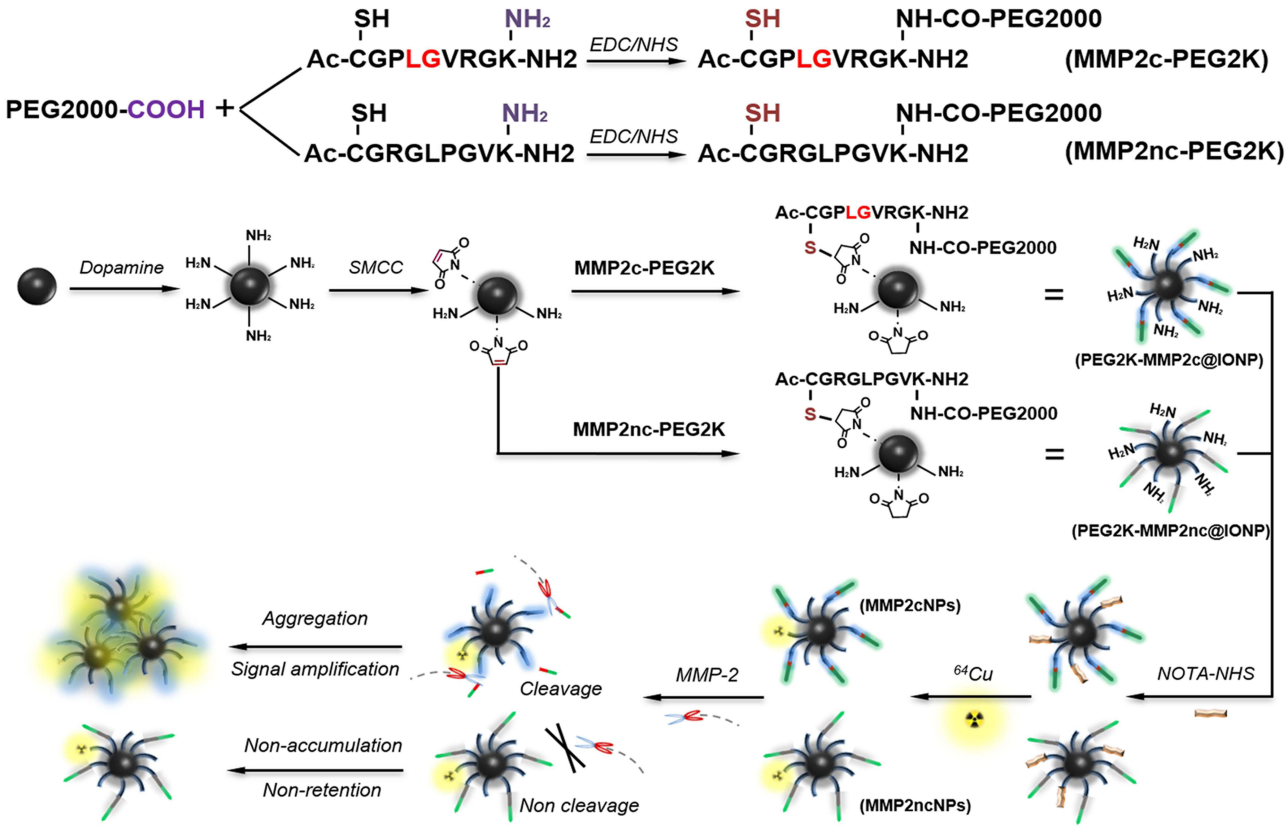

Figure 1 Schematic illustration of the synthesis of the smart multifunctional 64Cu-NOTA-IONP@MMP2c-PEG2K (MMP2cNPs) and the non-cleavable reference nanoparticles 64Cu-NOTA-IONP@MMP2c-PEG2K (MMP2ncNPs).

from Qiangyao organism. N-succinimidyl 4-(N-maleimidomethyl) cyclohexane-1-carboxylate (SMCC, Shanghai Haohong Biomedical Technology Co., Ltd.) and 1-ethyl-3-(3-dimethylaminopropyl) carbodiimide, hydrochloride (EDC) were purchased from Thermo Fisher Scientific. The PEG2K (PEG-carboxymethyl, MW 2000) was ordered from Sigma/Aldrich. Phosphate buffered saline (PBS, 0.01 M, pH 7.4) was obtained from Gibco/Invitrogen (Carlsbad, CA). All N-Fmoc-protected amino acids were purchased from Advanced ChemTech (Louisville, KY, USA). N, N'-dimethylformamide (DMF) and methylene chloride were ordered from Fisher Scientific (Fair Lawn, NJ, USA). Trifluoroacetic acid (TFA), O-benzotriazole-N, N, N', N'-tetramethyluronium hexafluorophosphate (HBTU), hydroxy-benzotriazole (HOBt), and 4-(2',4'-dimethoxyphenyl-Fmoc-aminomethyl)-phenoxy resin (Rink amide resin LS, 100–200 mesh, 1% DVB, 0.44 mmol/g) were purchased from Advanced Chemtech. Pyridine, acetic anhydride, acetic acid, and anhydrous ether were obtained from J.T.Baker (Phillipsburg, NJ, USA). Triisopropylsilane (TIPS), N-diisopropylethylamine (DIPEA), dithiothriotol (DTT), and 1, 2-ethanedithiol (EDT) were purchased from Aldrich (Milwaukee, WI, USA). Unless otherwise mentioned, all other chemicals were purchased from Sigma/Aldrich. Freeze dryer (Beijing Sihuan Scientific Instrument Factory Co., Ltd.); Fourier Infrared Spectrometer (Spectrum Two, Perkin-Elme, USA); Transmission Electron Microscope (JEM-1011, JEOL); Dynamic light-scattering particle size analyser (British Malvern Instrument Co., Ltd.); 3.0T magnetic resonance scanner (Trivo, Siemens). Deionized water was obtained from a Millipore Milli-DI Water Purification. Male CL57/BL6 mice were purchased from Charles River Laboratory (Wilmington, MA).

Preparation of SMCC-IONP

Firstly, magnetic Fe_3O_4 nanoparticles were first prepared by reference.[24] 10 mg Fe_3O_4 dispersed in 5 mL chloroform and 20 mg dopamine dissolved in 3 mL dimethyl sulfoxide were added into a flash bottle successively. The reaction mixture was vigorously stirred to form a homogeneous solution and was heated at 70°C for 2 h before being cooled down to room temperature. The amine-modified nanoparticles were precipitated out by adding 20 mL of ethyl ether and collected by centrifugation (4000 rpm for 8 min). The nanoparticles were then washed with ethanol, followed by centrifugation. Finally, the amine-modified nanoparticles (NH2-Fe/IONP) were redispersed in DMSO with nitrogen protection. Then, 1 mg of NH2-Fe/IONP was suspended in 1 mL of DMSO containing 5 mM SMCC. The solution was stirred for 2 h at room temperature. Typically, the SMCC-modified nanoparticles were precipitated out by adding 10 mL of ethyl ether and collected by centrifugation (4000 rpm for 8 min). The nanoparticles were then washed with ethanol, followed by centrifugation. The SMCC-modified nanoparticles (SMCC-IONP) were redispersed in DMSO with nitrogen protection.

Preparation of MMP-2 Cleavable Peptide (Ac-CGPLGVRGK-NH2), Mismatched Sequence (Ac-CGRGLPGVK-NH2)

See Supplementary Materials (Figure S2).

Preparation of MMP2c-PEG2K and MMP2nc-PEG2K

See Supplementary Materials (Figure S3-S4).

Synthesis of PEG2K-MMP2c@IONP and PEG2K-MMP2nc@IONP

The SMCC-IONP was redispersed in DMSO with nitrogen protection. 1 mg MMP2c-PEG2K or MMP2nc-PEG2K and 1 mg SMCC-IONP were added into 2 mL DMF and stirred at room temperature for 24 h under a nitrogen atmosphere. The product was washed several times with DMF and water under the action of a magnet, obtaining PEG2K-MMP -2c@IONP and PEG2K-MMP-2nc@IONP. And the water-soluble product PEG2K-MMP-2c@IONP or PEG2K-MMP -2nc@IONP was collected by centrifuge and re-dissolved in the water.

Radiolabeling

NOTA-NHS (20 eq) and PEG2K-MMP2c@IONP (1 eq) were mixed in water and incubated at room temperature overnight (pH = 8.5), and the unreacted materials were removed through the PD-10 column and dialysis membrane

(MWCO, 10,000). $^{64}CuCl_2$ ($t_{1/2}$ = 12.7 h) was obtained from the University of Wisconsin Madison, which was diluted 50:50 in ammonium acetate buffer (pH = 5.5) when received. PEG2K-MMP2c@IONP-NOTA was radiolabeled by the addition of ^{64}Cu, 5 mg of PEG2K-MMP2c@IONP-NOTA per millibecquerel of ^{64}Cu in 0.1N sodium acetate (pH = 5.5) buffer, and the mixture was incubated for 45 min at 40°C. PEG2K-MMP2c@IONP-NOTA was radiolabeled by the addition of desired radioactivity of conditioned $^{64}CuCl_2$ solution to 5 mg of PEG2K-MMP2c@IONP-NOTA in 0.1M sodium acetate (pH = 5.5) buffer, and the mixture was incubated for 30 min at 40°C. The solution was then purified using a PD-10 column with sterile phosphate-buffered saline as the mobile phase. The radioactive fractions containing ^{64}Cu-NOTA-IONP@MMP2c-PEG2K (MMP2cNPs) were collected for further in vitro and in vivo experiments. Similarly, the non-cleavable reference nanoparticles ^{64}Cu-NOTA-IONP@MMP2c-PEG2K (MMP2ncNPs) were synthesized as described above.

MR Phantom Study

See Supplementary Materials (Figure S5).

In vitro Stability

See Supplementary Materials (Figure S6–S7).

Particle Size and Zeta Potential Analysis

The hydrodynamic diameters of PEG2K-MMP2c@IONP-NOTA or PEG2K-MMP2nc@IONP-NOTA were determined using a Zetasizer Nano ZS90 DLS system equipped with a 633 nm-red laser at a detection angle of 90°. For each sample, three DLS measurements were conducted with a fixed 20 runs and each run lasts 10 seconds. The size of the nanoparticle was calculated from the diffusion coefficient of the particles using Stoke-Einstein equation by PCS software version. Zeta potential was measured as the particle electrophoretic mobility by means of laser microelectrophoresis in a thermostated cell. Every sample was diluted with phosphate buffer. Measurement was repeated three times and results were expressed as mean ± SEM deviation.

Transmission Electron Microscopy (TEM)

Microscopical analysis was carried out by transmission electron microscope (Philips CM-12 and Jeol JEM-1011) operating at 100 kV. The PEG2K-MMP2c@IONP-NOTA) or PEG2K-MMP2nc@IONP-NOTA were observed depositing a drop of their aqueous solution over carbon-coated copper grids and using as stain a 1% (w/w) aqueous solution of phosphotungstic acid. Magnetite nanoparticles were observed by placing a drop of chloroform dispersion onto a carbon-coated copper grid and dried at room temperature. The average size of crystallites was calculated by counting 100 individual nanoparticles.

Animals Experiments

The overall experimental procedure is shown in Figure S1. Macrophage-rich carotid artery plaques were induced in 40 CL57/BL6 mice by the following protocol. The mice were fed under standard animal room conditions (temperature 21 ±1°C; humidity 55–60%). Food and water were freely available throughout the experiments. Mice were fed with a high-fat diet containing 40% kcal fat, 1.25% (by weight) cholesterol and 0.5% (by weight) sodium cholate (Research Diets, Inc., USA). After 4 weeks of high-fat diet, mice were rendered diabetic by treatment of 5 daily intraperitoneal injections of streptozotocin (STZ), 40 mg/kg in citrate buffers (Sigma Aldrich). The serum glucose was measured from tail vein blood using a glucometer at day 5 of the STZ injections. If the glucose level was below 200 mg/dL, animals were injected with additional STZ for 3 consecutive days. At day 14 after initiation of STZ injection, the left common carotid artery was exposed by surgical incision and isolated by blunt glass minute hand, and then the left common carotid artery was completely ligated below the bifurcation with the use of 5–0 silk ligature (Ethicon) under 2% inhaled isoflurane as previously described.[25] The wound was closed by suture and the mice were allowed to recover on a warming blanket. All procedures were approved by the Administrative Panel on Laboratory Animal Care at Stanford University and the Experimental Animal Ethic Committee of Harbin Medical University (Animal Experimental Ethical Inspection Protocol

No. 2009104). The animal experiments were approved by the Ethics Committee of Harbin Medical University and performed in accordance with Regulations for the Administration of Affairs Concerning Experimental Animals (Order No. 2 of the State Science and Technology Commission of the People's Republic of China, 1988). In addition, all procedures were approved by the Animal Welfare Concerns of Laboratory Animal Care (APLAC) at Stanford University.

Magnetic Resonance Imaging

All the procedures were carried out in accordance with the in vivo animal protocols approved by the Institutional Animal Care and Use Committee at the Stanford University. All images were acquired on an MRI system (Magnex/Varian self-shielded 30 cm bore 7 Tesla magnet with a Research Resonance Instruments 9 cm bore gradient insert and the GE HealthCare "Micro"-Signa software environment). For all time points, the animal was anesthetized with an 1.5% isoflurane: air mixture, kept at 35–37°C with warm air flowing through the bore and the respiration was monitored. A 15-second localizer scan was conducted first followed by a pre-scan to allow for manual gradient shimming. For in vivo imaging, after localizing the ROI around the neck, a 3DSPGR-axial sequence (TE=1.7 ms, Flip Angle=10, FOV=30×30 mm^2, slice thickness=0.16 mm) and a 2DGRE sequence (TR/TE=50/1 ms, FOV=25×25 mm^2, Flip Angle=20, Band Width=31.25 mm, slice thickness=0.8 mm) were used before nanoparticles administration. In addition, a T2* two-dimensional gradient echo sequence (FSE) (TR/TE=3000/40 ms, Echo Train Length=16mm, Band Width=15.63 mm, FOV=28×28 mm^2, slice thickness=0.8 mm) was used for carotid arteries atherosclerotic plaques imaging pre- and 24 h after nanoparticles administration. Total in vivo imaging time was less than 60 min. The mice (n=4 for each group) were then removed from the scanner and allowed to recover in their cages.

The small-animal MRI data were analyzed using the commercially available DICOM image viewer OsiriX (http://www.osirix-viewer.com/). The imaging protocol was then repeated at pre- and 24 h post-injection. Continuous imaging on slices using the carotid bifurcation as a landmark allowed us to follow the contrast-to-noise ratio (CNR) in the carotid artery over time. Signal intensities were measured by manually drawing 4 regions of interest (ROI) within with carotid atherosclerotic plaque and the vessel lumen in CL57/BL6 mice. CNR was calculated for the signal intensity changes in similarly sized regions of interest located in the aortic lumen as well as within the vessel wall using the following equation: CNR= (mean value of wall signal−blood signal)/(standard deviation of the muscle signal).

Small Animal PET/CT Imaging

PET/CT imaging of CL57/BL6 mice with carotid atherosclerotic plaque was performed using a small animal PET/CT scanner (Siemens Inveon). Mice with carotid atherosclerotic plaque (n=4 for each group) were injected via the tail vein with approximately 2.96–3.7 MBq (80–100 μCi) of MMP2cNPs or MMP2ncNPs via tail vein. At 1, 2, 4, 12 and 24 h post-injection, mice were anesthetized with 2% isoflurane (5% for induction and 2% for maintenance in 100% O_2) and placed prone near the center of the field of view of the scanner for imaging experiments. CT images were acquired at 97 μm resolution with a 70 kV (40 μA) beam, 12 ms exposure, and 400 radial views over a 360-degree rotation. The images were reconstructed with a 2-dimensional ordered-subset expectation maximization algorithm with CT-based attenuation correction. Image files were analyzed using the vendor-supplied software Inveon Research Workspace (Preclinical Solutions; Siemens Healthcare Molecular Imaging). For each small-animal PET scan, 3-dimensional regions of interest (3D-ROIs) were drawn over the organs and tissues on decay-corrected whole-body images. The average radioactivity concentration in the ROI was calculated as percent of injected dose per gram tissue (%ID/g) from the mean pixel values within the ROI volume.

Biodistribution Studies

To test the MMP-2-cleavable specificity of MMP2cNPs in vivo, CL57/BL6 mice with carotid atherosclerotic plaque (n=3 for each group at different time points) were injected via the tail vein with 1.85–3.7 MBq (50–100 μCi) of MMP2cNPs or MMP2ncNPs via the tail vein and sacrificed at 1 h, 2 h, 4 h, 12 h and 24 h after injection and normal tissues of interest were removed and weighed, and their radioactivity levels were measured with a γ-counter. The radioactivity uptake in the plaques and normal tissues was calculated as a percentage of the injected radioactive dose per gram of tissue (% ID/g).

Histopathology

Tissues used for biodistribution analysis were stained for iron particle deposition using Prussian blue. The frozen sections were fixed with 4% glutaraldehyde, washed, incubated for 20 to 30 minutes with 2% potassium ferrocyanide (Perl reagent for Prussian blue staining) in 3.7% hydrochloric acid, washed again, and counterstained with nuclear fast red. Images of the entire carotid artery sections were captured with an automated scanning microscope equipped for wide-field fluorescence (Nano Zoomer Digital Pathology RS, Hamamatsu Photonics).

Immunohistochemistry

In order to determine the carotid artery plaques expressing MMP-2, double-color immunofluorescence analysis was performed as described previously. Briefly, frozen sections were incubated with PBS containing 1% normal donkey serum and 1% bovine serum albumin to reduce nonspecific reactions as previously described. Thereafter, the sections were further incubated in a combination of anti-F4/80 antibody (1:200 dilution, Abcam, ab6640, Rat monoclonal) and anti-MMP-2 antibody (1:100 dilution, Abcam, ab92536, Rabbit monoclonal). After incubation with Cy3-conjugated and Alexa Fluor 488-conjugated secondary antibody (1:500 dilution, Invitrogen, A-11008, A-11001) at room temperature for 60 min according to the manufacturer's protocol, the sections were captured with fluorescence microscope (IX71+DP72, Olympus).

Statistical Methods

All quantitative data are expressed as the mean ± SEM and analyzed by SPSS 27.0 software. The data obeys normal distribution based on Shapiro–Wilk normality test. Statistical analysis was performed using the Student's *t*-test for unpaired data. Differences were considered as statistically significant when $P < 0.05$.

Results

Synthesis and Characterization of MMP2cNPs and MMP2ncNPs

As shown in Figure 2A and B, the particle size of IONP was about 13.5 ± 3 nm. Meanwhile, the hydrated particle size of the magnetic particles modified with PEG2K-MMP2c or PEG2K-MMP2nc and NOTA significantly increased and dynamic light scattering measurement of PEG2K-MMP2c@IONP-NOTA or PEG2K-MMP2nc@IONP-NOTA particle sizes showed a mean hydrodynamic particle diameter of 30.5 ± 7.3 nm and 31.3 ± 11.2 nm, respectively (Figure 2A and B). The surface of the IONP nanoparticles is negatively charged, and the potential is −15.53 ± 1.80 mV. Due to large number of electronegative hydroxyl groups in PEG2K-MMP2c and NOTA, the zeta potential of PEG2K-MMP2c@IONP-NOTA is significantly reduced to −25.33 ± 1.10mV. Transmission electron microscopy results (Figure 2C) showed that the PEG2K-MMP2c@IONP-NOTA or PEG2K-MMP2nc@IONP-NOTA were well dispersed in water with a diameter of around 30 nm.

Identification of Carotid Atherosclerotic Plaque

MRI provided cross-sectional images of atherosclerotic lesions in the carotid artery. Stenosis within the artery was identified via the different signal intensities in T2 (FSE), and T1 (2DGRE) images of left carotid stenosis and confirmed using histopathology. Compared with contralateral right carotid artery, there was obvious stenosis within left collar artery observed on axial MRI image Figure 3A and B). On 3D-FLASH MR image, the longitudinal view showed that compared with the contralateral artery, the characteristic blood flow was significantly decreased and even vanished in the left carotid artery (Figure 3C). Moreover, the bright field anatomic image (Figure 3D) clearly displayed that there was a serious stenosis of the left common carotid artery at 3 months following surgery, while there was no stenosis of the contralateral right carotid artery.

In vivo PET/CT Imaging of MMP2cNPs

PET imaging is an essential approach to investigate nanomaterial biodistributions and atherosclerotic plaque accumulation. The serial static PET images of the mice injected with the MMP2cNPs or MMP2ncNPs were acquired. Representative coronal snapshots generated from whole-body in mice at different time points (1 h, 2 h, 4 h, 12 h and

A

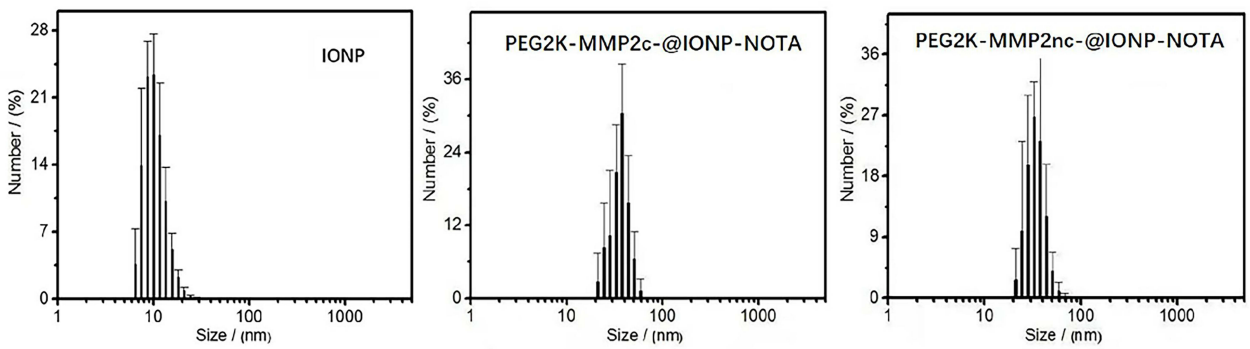

B

Formation	Size (nm)	Zeta potential (mv)
IONP	13.5±3	-15.53±1.80
PEG2K-MMP2c-@IONP-NOTA	30.5±7.3	-25.33±1.10
PEG2K-MMP2nc-@IONP-NOTA	31.3±11.2	-26.52±1.70

C

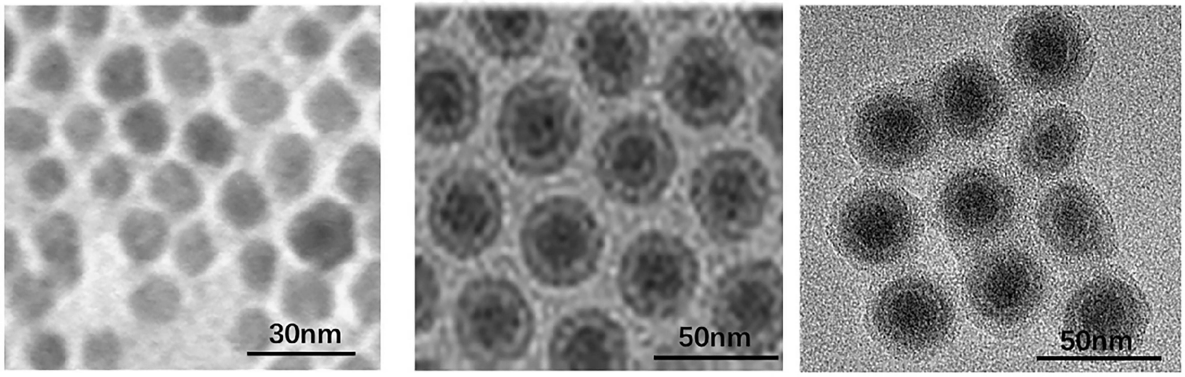

Figure 2 Preparation and characterization of MMP2cNPs and MMP2ncNPs. (**A** and **B**) Diameter and zeta potential of IONP, PEG2K-MMP2c@IONP-NOTA and PEG2K-MMP2nc@IONP-NOTA. (**C**) Transmission electron microscopy (TEM) image of IONP, PEG2K-MMP2c@IONP-NOTA and PEG2K-MMP2nc@IONP-NOTA.

24 h) after injection MMP2cNPs or MMP2ncNPs are shown in Figure 4A, and in vivo PET, CT, and PET/CT images of mice with carotid atherosclerotic plaques at 4 h after injection of MMP2cNPs are shown in Figure 5. The atherosclerotic lesion in the left carotid artery was clearly observed at 4 h after injection and demonstrated high contrast with low contralateral background (Figure 5), which persisted from 4 h to 12 h after injection of MMP2cNPs. However, there was no PET signal observed in carotid artery plaques from mice in the MMP2ncNPs group after injection. Moreover, biodistribution data confirmed the nonspecific uptake of the MMP2ncNPs by liver and kidneys, but little accumulation in other major organs such as brain, muscle, heart, suggesting the radiolabeled nanoparticle can be applied as a potential radioligand for the carotid atherosclerotic plaque PET imaging.

Ex vivo Biodistribution Studies

The ex vivo biodistribution of MMP2cNPs was performed to assess their in vivo behavior as potential PET/MRI imaging agents. Further quantification analysis of biodistribution, in general, agreed well with PET images result. The uptake of MMP2cNPs in carotid atherosclerotic plaque was 1.0 ± 0.26, 1.43 ±0.70, 3.06 ± 0.87, 1.96 ± 0.38, 0.21± 0.09%ID/g at 1 h, 2 h, 4 h, 12 h and 24 h after injection, respectively, while there was no remarkable uptake of MMP2ncNPs in carotid

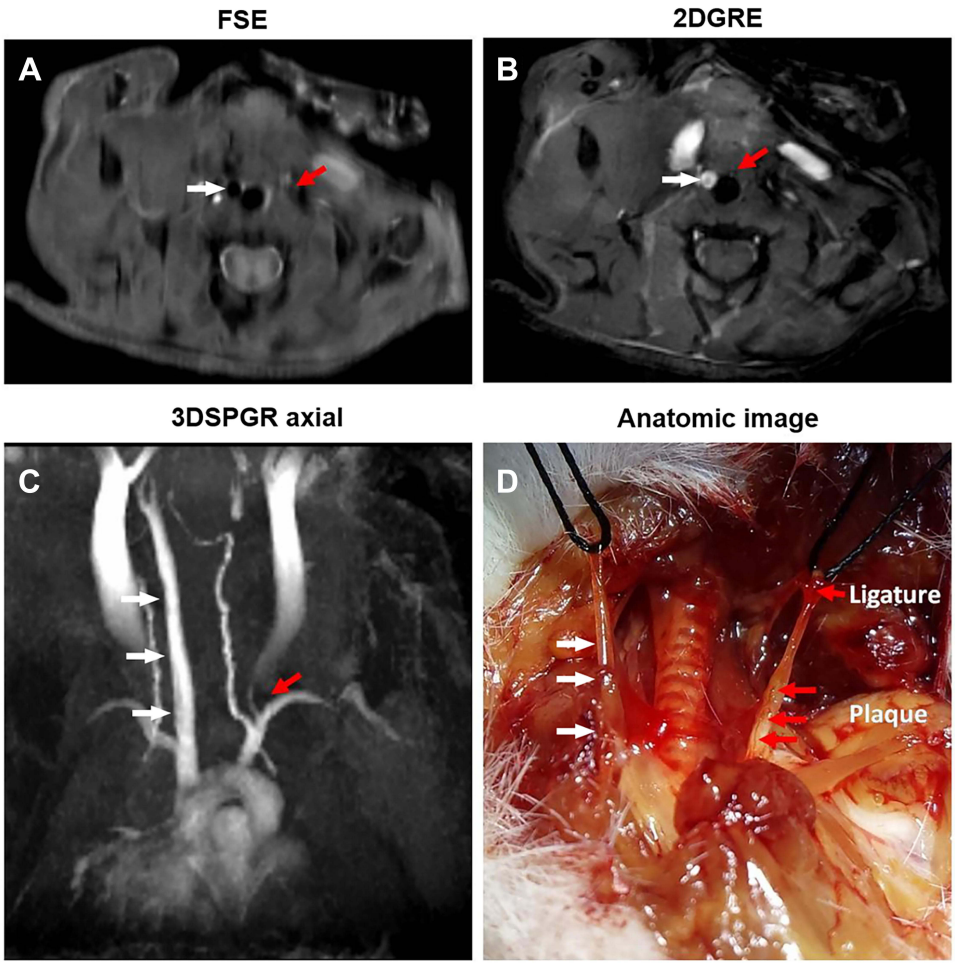

Figure 3 In vivo MR images acquired in carotid atherosclerotic plaques mice. (**A**) MRI provided cross-sectional images of atherosclerotic lesions in the carotid artery. Stenosis within the artery was identified via the different signal intensities in T2* two-dimensional gradient echo sequence (FSE), and (**B**) T1 (2DGRE) images of carotid atherosclerotic plaques (red arrow) and contralateral right carotid artery (white arrow). (**C**) On 3D-FLASH MR images, the longitudinal view showed an example of the characteristic blood flow that was significantly decreased in the left common carotid artery compared with the contralateral artery following surgery. (**D**) Bright-field anatomic image of vessel with carotid atherosclerotic plaques (red arrow) and control (white arrow).

atherosclerotic plaque from 1 h to 24 h after injection. Normal tissues such as common contralateral artery, brain, heart, and muscle exhibited much lower uptakes than carotid atherosclerotic lesion (Figure 4B). MMP2cNPs showed high accumulation in liver from 1 h to 24 h (20.50 ± 2.22, 20.43 ± 4.04, 23.84 ± 1.93, 31.69 ± 1.91, 17.73 ± 5.44%ID/g at 1 h, 2 h, 4 h, 12 h, and 24 h after injection, respectively) due to the liver clearance. The uptake in kidneys reached 18.91± 2.44% ID/g at 4 h and reduced to 4.42 ± 0.57% ID/g at 12 h after injection. Moreover, MMP2ncNPs also showed high accumulation in liver from 1 h to 24 h (19.33 ± 3.25, 22.42 ± 3.17, 25.38 ± 6.31, 26.69 ± 5.41, 15.73 ± 4.22%ID/g at 1 h, 2 h, 4 h, 12 h, and 24 h after injection, respectively). And the uptake of MMP2ncNPs in kidneys reached to maximum value (16.87± 2.23% ID/g) at 4 h and reduced to 3.82 ± 0.49% ID/g at 12 h after injection. In addition, quantification results showed that MMP2cNPs had high plaque-to-common contralateral artery ratios (Figure 4C), which bodes well for their application as in vivo molecular imaging agents.

In vivo MRI Imaging of MMP2cNPs

MRI is an essential medical imaging technique for atherosclerotic plaque diagnosis with high spatial resolution. To investigate atherosclerotic plaque and monitoring in vivo behavior, CL57/BL6 mice with carotid atherosclerotic plaques were intravenously administered with both active MMP2cNPs or inactive MMP2ncNPs and their T2*-weighted MR images were obtained at the predetermined time intervals. Representative T2-weighted MR transverse images of the

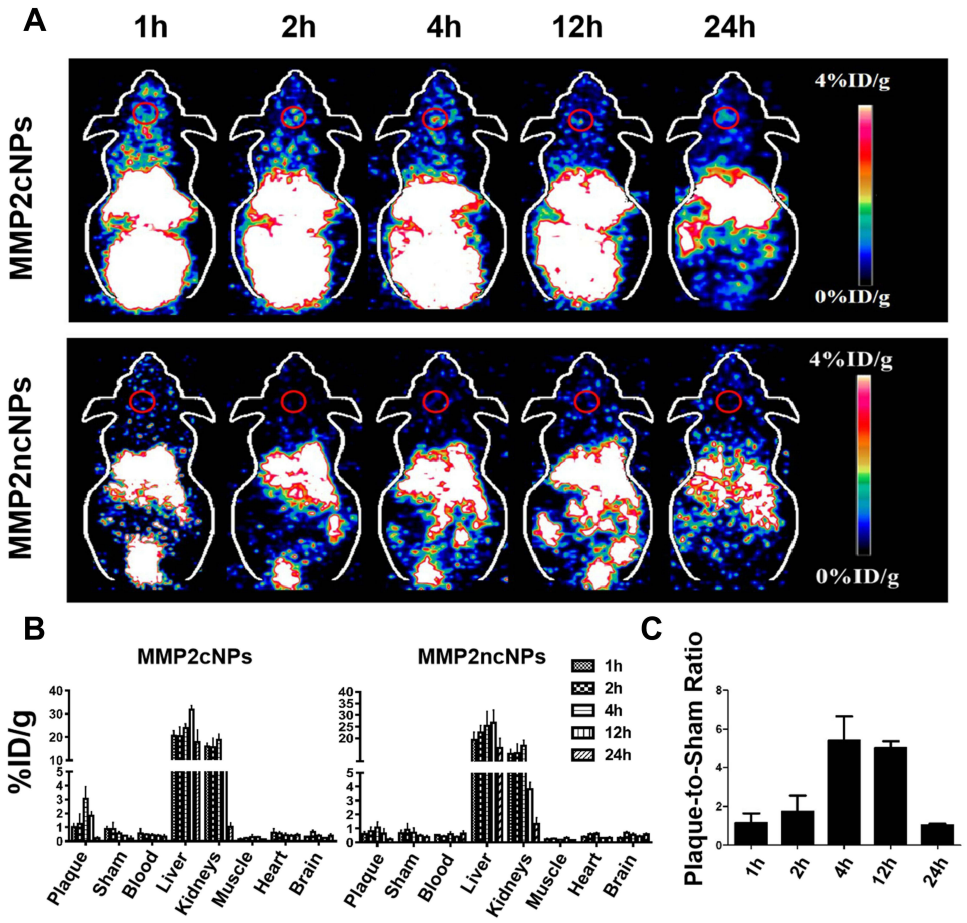

Figure 4 Small-animal PET images and quantification analysis results of MMP2cNPs. (**A**) Coronal PET images of mice models with carotid atherosclerotic plaques at 1 h, 2 h, 4 h, 12 h and 24 h after injection of MMP2cNPs or MMP2ncNPs. (**B**) Quantification analysis of radioactivity accumulation in selected organs at different time points after injection of MMP2cNPs and MMP2ncNPs, reported as %ID/g. (**C**) Quantification analysis of plaque-to-contralateral carotid artery ratios at different time points.

mouse carotid atherosclerotic plaque prior to and after injection of either cleavable or non-cleavable nanoprobes are shown in Figure 6A. The hypointense signals within the carotid atherosclerotic plaques were clearly observed after 24 h post-injection of cleavable MMP2cNPs but not the non-cleavable MMP2ncNPs nanoprobes. More importantly, the contrast effect induced by cleavable nanoprobes within the carotid atherosclerotic plaque was significantly higher than that of non-cleavable ones, indicating that there were more cleavable nanoprobes trapped within the carotid atherosclerotic plaque. Since the cleavable nanoprobes lost their water-solubility and tended to aggregate together, they diffused more slowly and had a longer retention time within the carotid atherosclerotic plaque tissues in comparison with those inactive nanoprobes, eventually leading to dramatic increases in the sensitivity and selectivity of MR imaging. These results implied that the smart MMP-2 cleavable nanoprobes as MR probes make it possible to actively reach and target the MMP-2 within atherosclerotic plaque in vivo.

The mean CNRs of the arterial ligation from pre-injection of MMP2cNPs and MMP2ncNPs groups were 18.65 ± 5.83 and 25.44 ± 8.39, respectively. Following MMP2cNPs injection, the CNR was significantly reduced in the MMP2cNPs group after 24 h post-injection (18.65 ± 5.83 vs 6.43 ± 2.56, $^{**}P<0.05$), but no markedly change in the MMP2ncNPs group (Figure 6B). The IONP are used as negative contrast agents and can cause hypointense signal intensities in T2*-weighted MR images. In our current study, the novelty MMP2cNPs was shown to aggregate within the plaques and consequently cause a clear T2* signal decrease on MRI, confirming the feasibility of MMP-2-targeted molecular imaging.

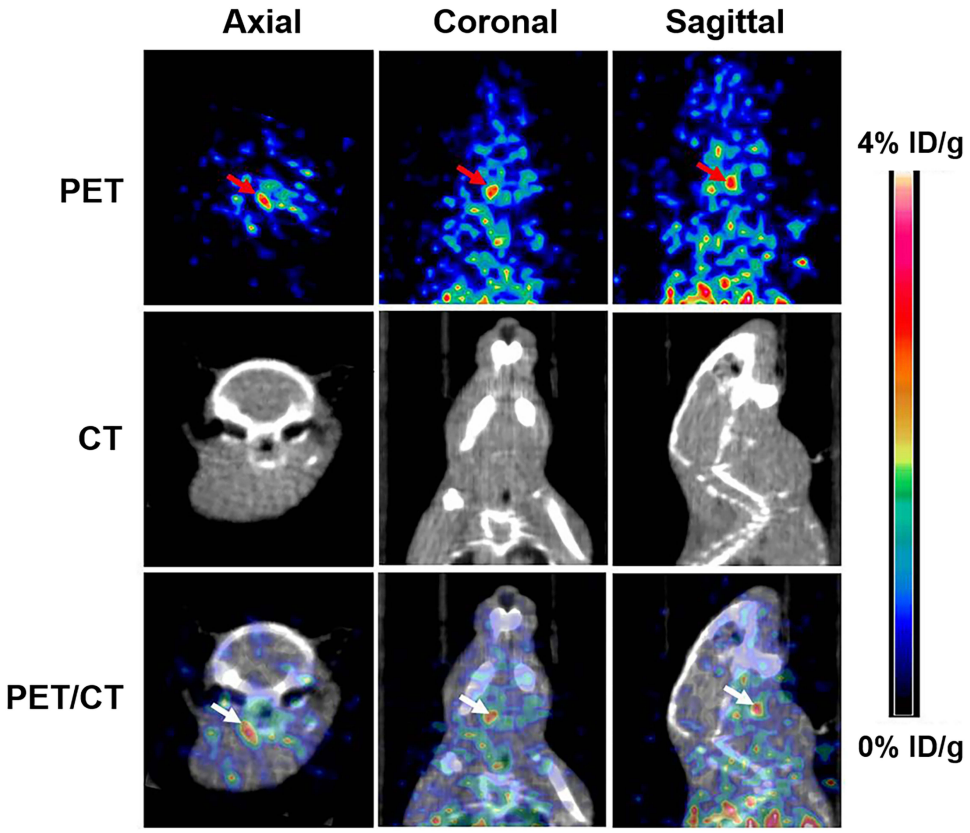

Figure 5 Small-animal PET images of MMP2cNPs in CL57/BL6 mice with carotid atherosclerotic plaque. The representative in vivo PET, CT, and PET/CT images of mice models with carotid atherosclerotic plaques at 4 h after injection of MMP2cNPs.

Immunofluorescence and Immunohistochemistry

To determine whether MMP-2 expression in the carotid atherosclerotic plaque was associated with macrophage infiltration, immunohistochemical staining was performed. F4/80^{+} stained macrophage of atherosclerotic lesions, and MMP-2 antibody identified the expression of MMP-2 in mouse carotid atherosclerotic plaques. The results revealed the distinct colocalization of both F4/80^{+} with MMP-2 in mouse carotid atherosclerotic plaques (Figure 7). To further confirm the precipitations of active MMP2cNPs within the mouse carotid atherosclerotic plaque, the vessel wall was stained with Perls stain (Figure 7). The staining results showed the co-localization of MMP2cNPs and MMP-2 enzyme within atherosclerotic plaques, while almost no deposition of MMP2ncNPs in plaques. Perls stain results in MMP2cNPs imaging group revealed a substantial iron accumulation within the plaques (indicated by the red arrows), whereas MMP2ncNPs group showed a small amount of iron staining within the plaques. Therefore, the immunofluorescence and immunohistochemistry results further indicated our novelty MMP2cNPs probe could be used to monitor the MMP-2 expression in the atherosclerosis plaque.

Discussion

Atherosclerosis, one of its most common drivers, is characterized by the gradual buildup of arterial plaque over time, which can ultimately lead to life-threatening conditions. Given the impact of the disease on public health, there is a great need for effective and noninvasive imaging modalities that can provide valuable information on its biological underpinnings during plaque development. Multiple new imaging modalities have been developed during the last century, which allowed in vivo molecular imaging of vascular inflammation in atherosclerosis, including fluorescence imaging, bioluminescence imaging, single photon emission computed tomography, PET, MRI, and CT.[26–30] It is reported that MMPs play important roles in the occurrence and development of cardiovascular diseases including atherosclerosis, myocardial infarction, and diabetic complication. Therefore, the evaluation of the activity of a specific subset of MMPs

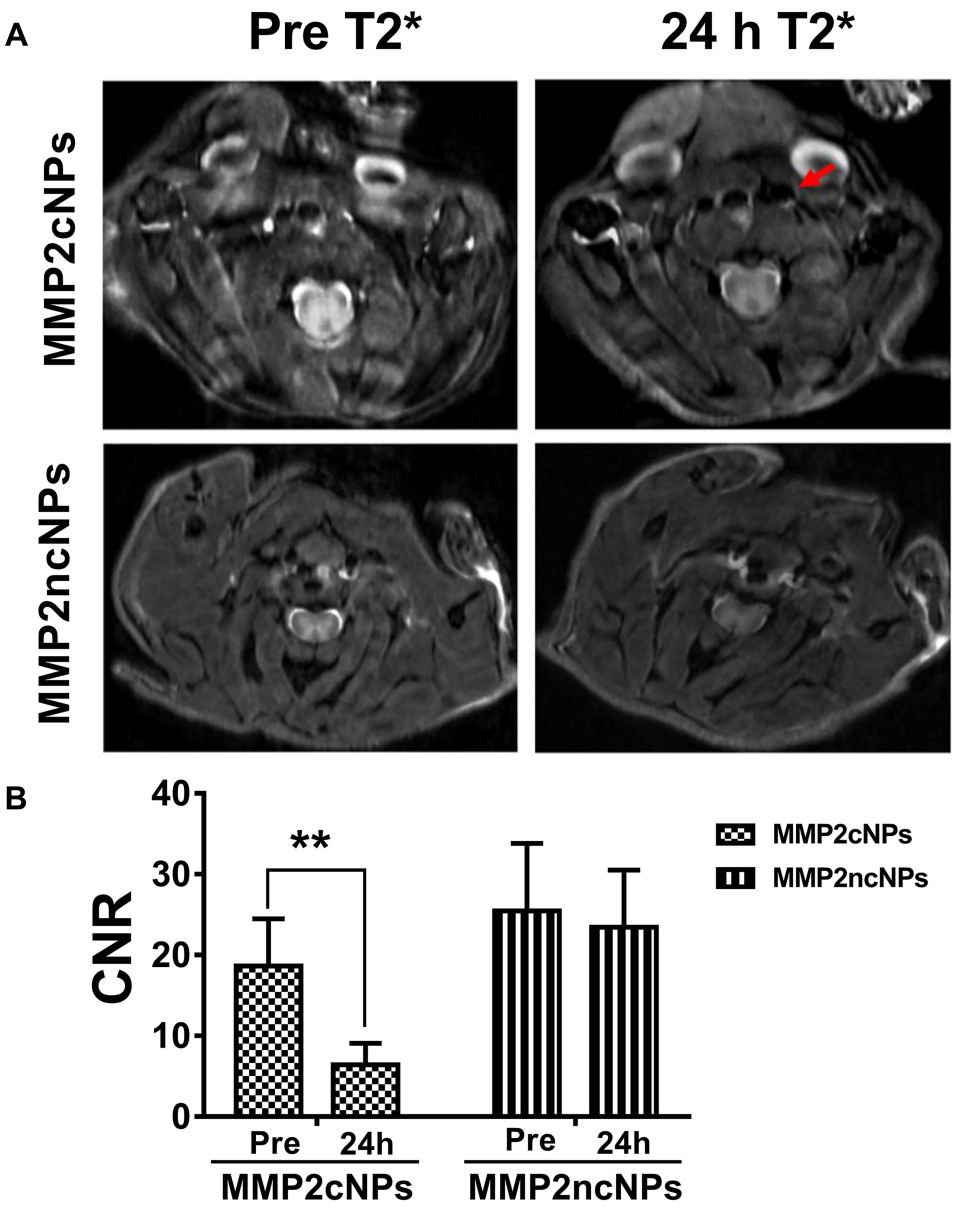

Figure 6 In vivo MRI of MMP2cNPs in CL57/BL6 mice with carotid atherosclerotic plaque. (**A**) In vivo CL57/BL6 mice with carotid atherosclerotic plaque MRIs obtained before and 24 h after administration of MMP2cNPs or MMP2ncNPs at a dose of 10 mg iron/kg (red arrow, cross section of the carotid artery). (**B**) Quantified data showed a significant reduction in CNR 24 h after administration of MMP2cNPs group, but not MMP2ncNPs, compared to before administration of MMP2cNPs or MMP2ncNPs (**P < 0.01).

in human diseases using clinically relevant molecular imaging techniques would be a powerful tool for the early diagnosis and assessment of the efficacy of therapy.[31]

In atherosclerosis, macrophages are the dominant leukocyte population, which play key roles in development of atherosclerotic plaques. Macrophage content has been used to evaluate atherosclerotic plaque burden in animal models and in humans. The macrophage and MMPs activity have potential for both reparative and destructive effects within the plaque, and are thus significant imaging and therapeutic targets. Early detection and diagnosis of macrophage-rich plaques are crucial for the prevention of its complications, such as acute myocardial infarction and ischemic stroke. For this reason, new molecular imaging methods that specifically target macrophages and MMPs in atherosclerotic unstable plaques and provide pivotal information on plaque location and stability are required.[32,33] In our study, the combination of high-fat diet and STZ-induced diabetes successfully generated macrophage-rich carotid-ligation lesions in CL57/BL6

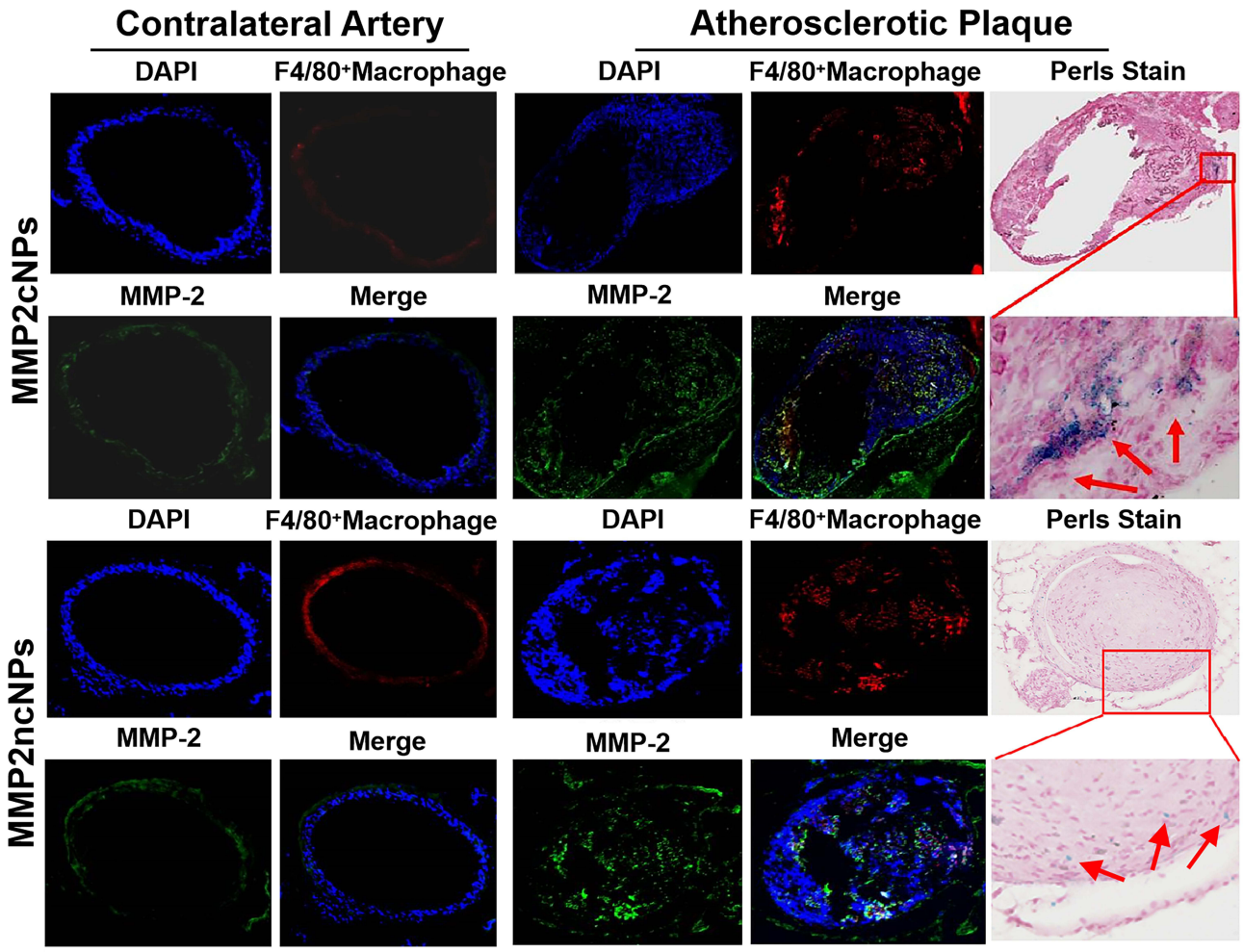

Figure 7 Localization of imaging targets to MMP-2 in atherosclerotic lesions. Dual immunofluorescent staining of MMP-2 (green) and F4/80+ (red) demonstrated partially colocalization within carotid artery atherosclerotic plaque. Yellow regions represent colocalization. Perls stain of iron was present in the plaque of carotid artery from MMP2cNPs and MMP2ncNPs group (red frame). Original magnification ×200.

mice, which provided an available carotid plaque model for in vivo imaging MMP-2 in plaques. In recent years, the potential of molecular imaging to characterize the processes involved in the initiation and progression of atherosclerotic lesions has been explored. In particular, radionuclide-based molecular imaging using PET and SPECT has been evaluated in preclinical and clinical studies.[34] Similarly, contrast-enhanced magnetic resonance imaging (MRI) and ultrasound are also areas of current research focus.[35]

Promising advance in the nanotechnology field over the past decade has resulted in the preclinical validation of nanoscale devices that target components of the atherosclerotic plaque at the cellular and molecular levels, including one of its prominent cell types, the macrophage. Iron oxide nanoparticle-enhanced MRI has been reported to be able to identify macrophage of atherosclerotic plaques in both in vivo animal and human studies. However, the non-specific contrast agents are taken up by activated macrophages in vulnerable plaques via pinocytosis, phagocytosis, or fluid-phase transport, which are inefficient processes. Without using smart enzyme digestion imaging nanoprobes in vivo, even increasing the dose of nanoparticles will not access high-quality imaging. Smart targeting of nanoparticles can be achieved by decorating them with a ligand, which can be cleaved by the known markers, like MMP-2, associated with vulnerable plaques.

In this study, in order to realize the noninvasive imaging of MMP-2 enriched carotid atherosclerotic lesions, we synthesized newly smart PET/MRI contrast agents, which was based on MMP-2 cleavable nanoparticles (MMP2cNPs). However, to our knowledge, in vivo combination of PET imaging and MRI for detecting vascular inflammation has not

fully been shown previously. In order to noninvasively assess plaque inflammation, Majmudar et al systematically developed a new polymeric nanoparticle consisting of cross-linked short chain dextrans (DNP), which was modified with desferoxamine for zirconium-89 radiolabeling (^{89}Zr-DNP) to realize PET/MR imaging.[36] The results showed that hybrid PET/MR imaging with a 13-nm DNP enabled noninvasive assessment of inflammation in experimental atherosclerotic plaques.

Molecular imaging is a rapidly developing field, with the use of hybrid technology scanners or multi-modality imaging method for in vivo investigations covering a broad spectrum of cardiovascular diseases. PET imaging has superiority for detection of cellular and molecular targets because it is the most sensitive noninvasive clinical imaging technology and permits quantitative analysis. MRI, as a pivotal modality for in vivo imaging the cardiovascular diseases, may prove to be particularly useful in conjunction with PET imaging. Sparse cellular or molecular targets can be accurately quantitated by in vivo PET imaging, whereas MRI possesses higher solution, high-contrast, and time-resolved cardiovascular imaging without additional radiation exposure.[36–38] In the current study, in order to in vivo monitor the MMP-2 within mouse carotid atherosclerotic lesions, we developed a novel smart PET/MRI contrast agent based on MMP-2 cleavable nanoparticles. Firstly, in the mouse carotid atherosclerotic lesions model, the CL57/BL6 mice were treated by 5 daily intraperitoneal injections of streptozotocin (STZ) and ligation of left common carotid artery below the bifurcation combined with a cholesterol-enriched diet led to neointimal thickening, with lesions composed of many macrophages (Figure S1). And the lumen was almost blocked because of the proliferation of neointimal tissue, which was imaged by MRI to confirm the presence of lesions at the injury site before in vivo PET/MRI molecular imaging (Figure 3). Previous studies have indicated that it is possible to in vivo monitor atherosclerotic lesions by using MRI contrast agent USPIO.[39,40] And the PEG-coated iron oxides are known to reduce plasma protein binding, delay clearance by the reticuloendothelial system and increase particle circulation times. In our current study, the magnetic IONP base material has been derivatized with NOTA for the nuclear tracer ^{64}Cu and the MMP-2-cleavable peptide modified with PEG2000, yielding a multi-modality reporter MMP2cNPs for in vivo PET/MR molecular imaging. The PET imaging data in this current study showed that after the intravenous injection of the MMP2cNPs or MMP2ncNPs with the same dose, the animals were scanned through a micro-PET imaging system, the PET signal could not be clearly distinguished at the plaques site among the mice with the MMP2cNPs or MMP2ncNPs at 1h after the intravenous injection. However, at 4 h, the MMP2cNPs displayed predominant mouse carotid plaque uptake as compared to the contralateral right carotid artery, but the MMP2ncNPs showed no marked accumulation within the mouse carotid plaque from beginning to end after the intravenous injection (Figure 4). In addition, the MR imaging results in our study showed that hypointense signals within the carotid atherosclerotic plaque were clearly observed after 24 h post-injection of active MMP2cNPs but not inactive MMP2ncNPs nanoprobes (Figure 6). We also found that MMP2cNPs obviously accumulated in mouse carotid plaque, because the MMP-2 cleavable peptide of MMP2cNPs was cut by the MMP-2 secreted from macrophages in atherosclerotic plaques. The immunohistochemistry data confirmed the colocalization of MMP-2 and F4/80^{+} expression and iron oxide nanoparticles deposition within mouse carotid plaque models (Figure 7). According to the above experimental results, our study indicated that the constructed probe could reflect the activity of MMP-2 within plaque and was considered as a promising target for molecular PET/MRI of atherosclerosis. Thus, we have provided another targeted molecular imaging of USPIO-based contrast agents for detecting and monitoring the progression of the plaque lesions. The advantage of PET/MRI was benefiting from the high anatomical spatial resolution and good soft tissue contrast of MRI and the unparalleled sensitivity and noninvasive functional molecular imaging of PET. Based on this, more plaque details can be found by PET, and more information about plaque spatial localization can be found by MRI. As a research tool, the ability to detect MMP-2 in atherosclerotic plaques using in vivo PET/MR imaging provides a valuable biomarker to assess plaque stability, which would be a new diagnostic tool for clinicians. So, our data highlight the advantages of combining both modalities in assessment of atherosclerosis plaque.

Study Limitations

In our study, there exist some limitations. Firstly, no matter in the previous related research or the current study, the IONP materials are inclined to accumulate in the liver and kidneys. This is an unavoidable problem in IONP molecular imaging field, which is our future direction to resolve this conundrum. Secondly, we could not acquire PET/MR multimodal imaging data simultaneously, because there was no micro-PET/MR integrated imaging instrument at that time. Finally, it remains to be seen whether our novel smart probe accumulated in plaques could further trigger the inflammatory and

worsen the plaque stability. Given these practical difficulties, further investigation would be performed in our future studies.

Conclusion

Current development in multimodality imaging allows researchers to gather vital molecular and cellular aspects of atherosclerosis biology in vivo, providing attractive and practical tools for early and accurate diagnosis of atherosclerotic vulnerable plaque. MMPs are fatal components in the formation and development of atherosclerotic plaque whose identification and detection are still a challenge using conventional imaging methods. In this current study, we have synthesized a novel MMP-2 cleavable PET/MR imaging contrast agent and demonstrated the feasibility of nanoparticle-facilitated hybrid PET/MRI of MMP-2 in mouse carotid atherosclerotic plaques. Whether the probe of MMP2cNPs can serve as a full potential vector in the assessment of atherosclerotic plaque still requires further investigation.

Data Sharing Statement

Data sharing is not applicable to this article as no datasets were generated or analysed during the current study.

Ethics Approval and Consent to Participate

All procedures were approved by the Administrative Panel on Laboratory Animal Care at Stanford University and the Experimental Animal Ethic Committee of Harbin Medical University (Animal Experimental Ethical Inspection Protocol No. 2009104).

Acknowledgments

This work was supported, in part, by the National Natural Science Foundation of China (81671746, 81827806, 81571747, 81771907), and the Office of Science (BER), US Department of Energy (DE-SC0008397), Postdoctoral Science Foundation of Heilongjiang Province (LBH-Q19037), Key research and development project of Shanxi Province (Nos. 201703D321015-3), Science and technology innovation team project (NO. 201705D131026), Scientific and technological achievements transformation project of Shanxi Province (No. 201704D131006) and Shanxi Province Science Foundation for Youths (No. 201701D221257), the doctoral fund of Shanxi Cancer Hospital (No. 2017A01).

Disclosure

The patent issued relevant to the work. Patent authors: Yingfeng Tu, Jiannan Dai, Huai Yu, Jinwei Tian, Lulu Li. Patent number: CN110302400A. Patent title: Structure and application of PET/MRI multimodal molecular imaging nanoprobes for early diagnosis of vulnerable atherosclerotic plaques. The authors report no other conflicts of interest in this work.

References

1. Benjamin EJ, Blaha MJ, Chiuve SE, et al. Heart disease and stroke statistics-2017 update: a report from the American Heart Association. *Circulation*. 2017;135(10):e146–e603.
2. Zhang J, Zu Y, Dhanasekara CS, et al. Detection and treatment of atherosclerosis using nanoparticles. *Wiley Interdiscip Rev Nanomed Nanobiotechnol*. 2017;9(1):1. doi:10.1002/wnan.1412
3. Noukeu LC, Wolf J, Yuan B, Banerjee S, Nguyen KT. Nanoparticles for detection and treatment of peripheral arterial disease. *Small*. 2018;14(32): e1800644. doi:10.1002/smll.201800644
4. Montiel SM, Lassalle VL. Magnetic iron oxide nanoparticles as novel and efficient tools for atherosclerosis diagnosis. *Biomed Pharmacother*. 2017;93:1098–1115. doi:10.1016/j.biopha.2017.07.012
5. Beldman TJ, Senders ML, Alaarg A, et al. Hyaluronan nanoparticles selectively target plaque-associated macrophages and improve plaque stability in atherosclerosis. *Acs Nano*. 2017;11(6):5785–5799. doi:10.1021/acsnano.7b01385
6. Ai F, Ferreira CA, Chen F, Cai W. Engineering of radiolabeled iron oxide nanoparticles for dual-modality imaging. *Wiley Interdiscip Rev Nanomed Nanobiotechnol*. 2016;8(4):619–630. doi:10.1002/wnan.1386
7. Bejarano J, Navarro-Marquez M, Morales-Zavala F, et al. Nanoparticles for diagnosis and therapy of atherosclerosis and myocardial infarction: evolution toward prospective theranostic approaches. *Theranostics*. 2018;8(17):4710–4732. doi:10.7150/thno.26284
8. Moriya J. Critical roles of inflammation in atherosclerosis. *J Cardiol*. 2019;73(1):22–27. doi:10.1016/j.jjcc.2018.05.010
9. Bentzon JF. Targeting Inflammation in atherosclerosis. *J Am Coll Cardiol*. 2016;68(25):2794–2796. doi:10.1016/j.jacc.2016.11.005
10. Zhang X, Liu C, Nepal S, et al. A hybrid approach for scalable sub-tree anonymization over big data using MapReduce on cloud. *J Comput Syst Sci*. 2014;80(5):1008–1020.

11. Seifert R, Kuhlmann MT, Eligehausen S, et al. Molecular imaging of MMP activity discriminates unstable from stable plaque phenotypes in shear-stress induced murine atherosclerosis. *PLoS One*. 2018;13(10):e0204305. doi:10.1371/journal.pone.0204305
12. Dhillon OS, Khan SQ, Narayan HK, et al. Matrix metalloproteinase-2 predicts mortality in patients with acute coronary syndrome. *Clin Sci*. 2009;118(4):249–257. doi:10.1042/CS20090226
13. Dhanasekara CS, Zhang J, Nie S, et al. Nanoparticles target intimal macrophages in atherosclerotic lesions. *Nanomedicine*. 2021;32:102346. doi:10.1016/j.nano.2020.102346
14. Zhao Y, Xie R, Yodsanit N, et al. Biomimetic fibrin-targeted and H2O2-responsive nanocarriers for thrombus therapy. *Nano Today*. 2020;35:1. doi:10.1016/j.nantod.2020.100986
15. Burtea C, Ballet S, Laurent S, et al. Development of a magnetic resonance imaging protocol for the characterization of atherosclerotic plaque by using vascular cell adhesion molecule-1 and apoptosis-targeted ultrasmall superparamagnetic iron oxide derivatives. *Arterioscler Thromb Vasc Biol*. 2012;32(6):e36–48. doi:10.1161/ATVBAHA.112.245415
16. Chen H, Chen L, Liang R, Wei J. Ultrasound and magnetic resonance molecular imaging of atherosclerotic neovasculature with perfluorocarbon magnetic nanocapsules targeted against vascular endothelial growth factor receptor 2 in rats. *Mol Med Rep*. 2017;16(5):5986–5996. doi:10.3892/mmr.2017.7314
17. Pedersen SF, Sandholt BV, Keller SH, et al. 64Cu-DOTATATE PET/MRI for detection of activated macrophages in carotid atherosclerotic plaques: studies in patients undergoing endarterectomy. *Arterioscler Thromb Vasc Biol*. 2015;35(7):1696–1703. doi:10.1161/ATVBAHA.114.305067
18. Yao Y, Li B, Yin C, et al. A folate-conjugated dual-modal fluorescent magnetic resonance imaging contrast agent that targets activated macrophages in vitro and in vivo. *J Biomed Nanotechnol*. 2016;12(12):2161–2171. doi:10.1166/jbn.2016.2316
19. Nahrendorf M, Zhang H, Hembrador S, et al. Nanoparticle PET-CT imaging of macrophages in inflammatory atherosclerosis. *Circulation*. 2008;117(3):379–387. doi:10.1161/CIRCULATIONAHA.107.741181
20. Kiugel M, Hellberg S, Kakela M, et al. Evaluation of [(68)Ga]Ga-DOTA-TCTP-1 for the detection of metalloproteinase 2/9 expression in mouse atherosclerotic plaques. *Molecules*. 2018;23(12):1. doi:10.3390/molecules23123168
21. Yan F, Yang W, Li X, et al. Magnetic resonance imaging of atherosclerosis using CD81-targeted microparticles of iron oxide in mice. *Biomed Res Int*. 2015;2015:758616. doi:10.1155/2015/758616
22. Yang CT, Ghosh KK, Padmanabhan P, et al. PET-MR and SPECT-MR multimodality probes: development and challenges. *Theranostics*. 2018;8(22):6210–6232. doi:10.7150/thno.26610
23. Su T, Wang YB, Han D, et al. Multimodality imaging of angiogenesis in a rabbit atherosclerotic model by GEBP11 Peptide targeted nanoparticles. *Theranostics*. 2017;7(19):4791–4804. doi:10.7150/thno.20767
24. Chen M, Xiong F, Ma L, et al. Inhibitory effect of magnetic Fe3O4 nanoparticles coloaded with homoharringtonine on human leukemia cells in vivo and in vitro. *Int J Nanomedicine*. 2016;11:4413–4422. doi:10.2147/IJN.S105543
25. Terashima M, Ehara S, Yang E, et al. In vivo bioluminescence imaging of inducible nitric oxide synthase gene expression in vascular inflammation. *Mol Imaging Biol*. 2011;13(6):1061–1066. doi:10.1007/s11307-010-0451-5
26. Chaudhry F, Kawai H, Johnson KW, et al. Molecular imaging of apoptosis in atherosclerosis by targeting cell membrane phospholipid asymmetry. *J Am Coll Cardiol*. 2020;76(16):1862–1874. doi:10.1016/j.jacc.2020.08.047
27. Lariviere M, Lorenzato CS, Adumeau L, et al. Multimodal molecular imaging of atherosclerosis: nanoparticles functionalized with scFv fragments of an anti-alphaIIbbeta3 antibody. *Nanomedicine*. 2019;22:102082. doi:10.1016/j.nano.2019.102082
28. Lariviere M, Bonnet S, Lorenzato C, et al. Recent advances in the molecular imaging of atherosclerosis. *Semin Thromb Hemost*. 2020;46(5):563–586. doi:10.1055/s-0039-1701019
29. Lobatto ME, Binderup T, Robson PM, et al. Multimodal positron emission tomography imaging to quantify uptake of (89) Zr-labeledliposomes in the atherosclerotic vessel wall. *Bioconjug Chem*. 2020;31(2):360–368. doi:10.1021/acs.bioconjchem.9b00256
30. Werner RA, Bengel FM, Derlin T. Emerging molecular targets for imaging of atherosclerotic plaque using positron emission tomography. *Curr Radiopharm*. 2021;14(3):173–183. doi:10.2174/1874471013666200505102353
31. Rangasamy L, Geronimo BD, Ortin I, et al. Molecular imaging probes based on matrix metalloproteinase inhibitors (MMPIs). *Molecules*. 2019;24:16. doi:10.3390/molecules24162982
32. Toczek J, Bordenave T, Gona K, et al. Novel matrix metalloproteinase 12 selective radiotracers for vascular molecular imaging. *J Med Chem*. 2019;62(21):9743–9752. doi:10.1021/acs.jmedchem.9b01186
33. Gona K, Toczek J, Ye Y, et al. Hydroxamate-based selective macrophage elastase (MMP-12) inhibitors and radiotracers for molecular imaging. *J Med Chem*. 2020;63(23):15037–15049. doi:10.1021/acs.jmedchem.0c01514
34. Hu Y, Liu G, Zhang H, et al. A comparison of [(99m)Tc]Duramycin and [(99m)Tc]Annexin V in SPECT/CT imaging atherosclerotic plaques. *Mol Imaging Biol*. 2018;20(2):249–259. doi:10.1007/s11307-017-1111-9
35. Evans RJ, Lavin B, Phinikaridou A, et al. Targeted molecular iron oxide contrast agents for imaging atherosclerotic plaque. *Nanotheranostics*. 2020;4(4):184–194. doi:10.7150/ntno.44712
36. Majmudar MD, Yoo J, Keliher EJ, et al. Polymeric nanoparticle PET/MR imaging allows macrophage detection in atherosclerotic plaques. *Circ Res*. 2013;112(5):755–761. doi:10.1161/CIRCRESAHA.111.300576
37. Pedersen SF, Ludvigsen TP, Johannesen HH, et al. Feasibility of simultaneous PET/MR in diet-induced atherosclerotic minipig: a pilot study for translational imaging. *Am J Nucl Med Mol Imaging*. 2014;4(5):448–458.
38. Gholami YH, Yuan H, Wilks MQ, et al. A radio-nano-platform for T1/T2 dual-mode PET-MR Imaging. *Int J Nanomedicine*. 2020;15:1253–1266. doi:10.2147/IJN.S241971
39. Zheng KH, Schoormans J, Stiekema L, et al. Plaque permeability assessed with DCE-MRI associates with USPIO uptake in patients with peripheral artery disease. *JACC Cardiovasc Imaging*. 2019;12(10):2081–2083. doi:10.1016/j.jcmg.2019.04.014
40. Sha T, Qi C, Fu W, et al. Experimental study of USPIO-enhanced MRI in the detection of atherosclerotic plaque and the intervention of atorvastatin. *Exp Ther Med*. 2016;12(1):141–146. doi:10.3892/etm.2016.3266